Study of Sound Waves in Fluidized Bed using CFD-DEM Simulations

H. A. Khawaja
hassan.a.khawaja@uit.no
Process and Gas Group
Department of Engineering & Safety
UiT-The Arctic University of Norway
9037, Langnes, Tromsø, Norway

Abstract

The speed of sound waves is investigated using CFD-DEM numerical simulations. Appropriate initial and boundary conditions are applied to capture the phenomenon. The effect of varying the height of the bed is also studied. The results of the simulations matched those from literature. The pressure and particle velocity profiles from the simulation showed the oscillatory behavior. Functions (based on a damped standing wave) were fitted to these, which allowed them to be stated in time and space variables. These fitted functions were substituted to the linearized governing equations for the two-phase flow. Using these assumed solutions allowed a new relationship to be derived for the speed of sound and damping in the system. It is concluded that the damping in the system is due to the effective bulk viscosity of the solid phase, which arises from the particle viscosity.

1 Introduction

The presence of particles in a gas phase (as in a fluidized bed) is known to affect the propagation of sound waves through the continuous phase. Cahan (1990) studied sound waves by sprinkling lycopodium seeds into an oscillating column of air within a tube to identify the nodes of a standing wave. It was found that the sound waves diminished in the presence of particles and that the speed of sound measured changed from its theoretical value in air. Later, Mallock (1910) studied the velocity of sound in liquid-gas mixtures such as froths. The results also showed that the speed of sound differed from the value in gas in a similar manner to that of the gas-particle mixture studied by Cahan (1990). Similarly, Roy, Davidson, and Tuponogov

(1990) studied the speed of sound in a gas-fluidized bed. They cross-correlated the pressure signal at different heights of the bed to detect the speed of the moving disturbance, as well as measuring the frequency of the standing wave after a disturbance had been introduced to infer wave speed. It was found that the speed of sound is significantly lower in the gas-particle medium.

The velocity of a sound wave in a continuous compressible medium is given by Lamb (1963) as shown in Equation (1),

$$u_s = \sqrt{\frac{dp}{d\rho}} \tag{1}$$

where u_s is the speed of sound and $dp/d\rho$ is the rate of change of pressure with bulk density.

To apply the given relationship (Equation (1)) to a two-phase mixture of gas and particles, a number of assumptions need to be made, as provided by Roy et al. (1990) and later acknowledged by H. T. Bi, Grace, and Zhu (1995) and Hsiaotao T. Bi (2007). These assumptions are also given by Mallock (1910), Tangren, Dodge, and Seifert (1949) and Campbell and Pitcher (1958).

1. The particles and gas move together (i.e. homogenous rather than separated flow),
2. The gas is compressible and obeys the ideal gas law,
3. The particles are incompressible,
4. The particulate matter and gas are isothermal.

The assumption that the gas and particles are in an isothermal state can be justified by computing the time required for solid and gas to attain the same temperature as discussed by Roy et al. (1990). This assumption might not be valid in fluidized beds with larger particles because increasing the size of particle increases the time constant value, hence, increasing the time taken by the system to reach thermal equilibrium. A similar conclusion is reached by Turton, Fitzgerald, and Levenspiel (1989) and Kunii and Levenspiel (1991).

Roy et al. (1990) derived an expression for the speed of sound in a homogenous two-phase medium as shown in Equation (2),

$$u_s = \sqrt{\frac{\rho_g R T_g}{\epsilon\left(\rho_s(1-\epsilon) + \rho_g \epsilon\right)}} \quad (2)$$

where ρ_s is the density of solids, ρ_g is the density of gas, ϵ is the void fraction, T_g is the absolute gas temperature and R is the specific gas constant.

It is to be noted that Equation (2) is only valid when the value of voidage is less than one ($\epsilon < 1$). Roy et al. (1990) demonstrated experimentally that the speed of sound in a fluidized mixture of sand and air is typically 1/30 of the speed of sound in air. Similar results are reported by H. T. Bi et al. (1995), who found the speed of sound to be 10 m/s in a fluidized mixture of air and fine particles (50 µm diameter with a density of 1580 kg/m^3).

Roy et al. (1990) also suggested a theoretical damping time relationship, derived by assuming a system of a mass attached to a spring with viscous damping as shown in Equation (3),

$$\tau = \frac{2g}{\omega^2 U_{mf}} \quad (3)$$

where τ is the damping time, g is the gravity constant, ω is the angular frequency of the oscillations and U_{mf} is the minimum fluidization velocity.

In this work, the speed of sound in the fluidized medium is verified through experiment and CFD-DEM (Computational Fluid Dynamics – Discrete Element Modelling) numerical simulations. The results are also analyzed analytically, revealing the importance of particle viscosity in the damping of sound waves in the fluidized bed.

2 Experimental verification of speed of sound in a fluidized medium

An experiment was set up to demonstrate the standing wave which can be created in a fluidized medium. Roy et al. (1990) associated standing waves in the fluidized medium with the speed of sound. Their explanation takes into account a case analogous to an organ pipe, with one end closed and the other open. A simple experiment was set up to observe the same behavior, as shown in Figure 1.

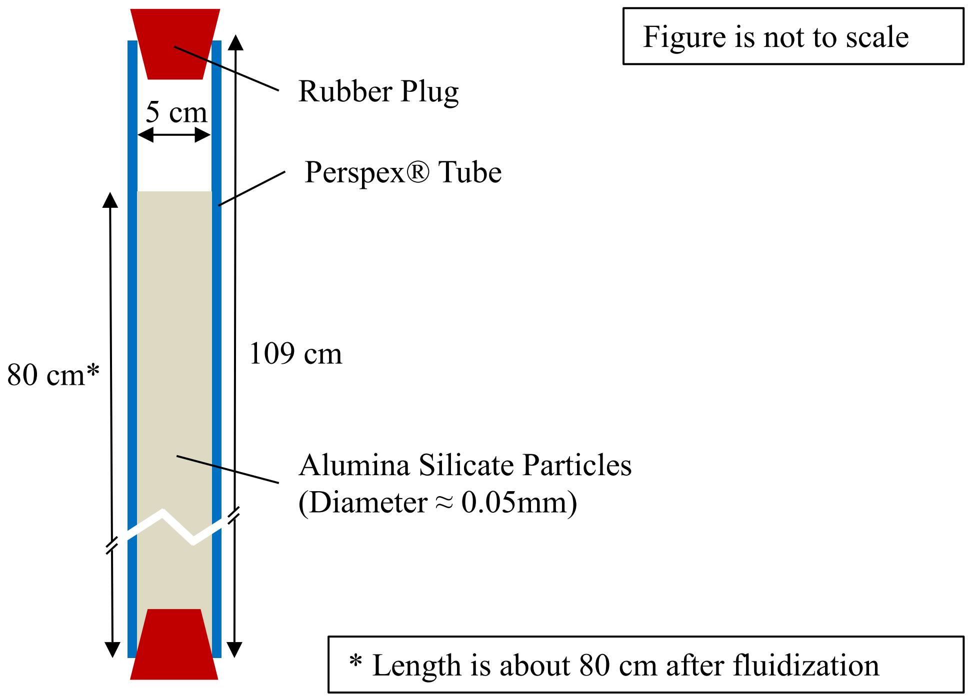

Figure 1: Experiment setup to study the standing wave in a fluidized bed

The experimental setup consists of a Perspex® tube with an internal diameter of 5 cm and an external diameter of 6 cm. The two ends of the tube are sealed with rubber plugs. The tube is filled with alumina silicate particles (diameter ≈ 50 µm). These particles are fluidized by rotating the tube vertically for a few 360-degree rotations. As the result of rotation, the particles are exposed to centrifugal force, building a relative velocity between gas and particles. This causes the particles to fluidize, i.e. the powder gas mixture becomes free-flowing, and a horizontal level 'free surface at meniscus' forms, regardless of the tilt of the tube. In addition, a significant expansion in the fluidized bed is noted before and after fluidization. Once fluidized, an impact load is induced in the fluidized medium by striking the tube on the ground. This induces vertical oscillations in the fluidized medium, corresponding to the standing wave in the medium. The frequency of these oscillations is noted by making a video of the meniscus of the fluidized medium at 30 Hz using Sony Handycam DCR-HC14E. A .wmv clip was captured and converted into image files; the captured images were observed to measure the wave frequency. Figure 2 shows the oscillations in the fluidized medium as captured using the above-described experimental setup.

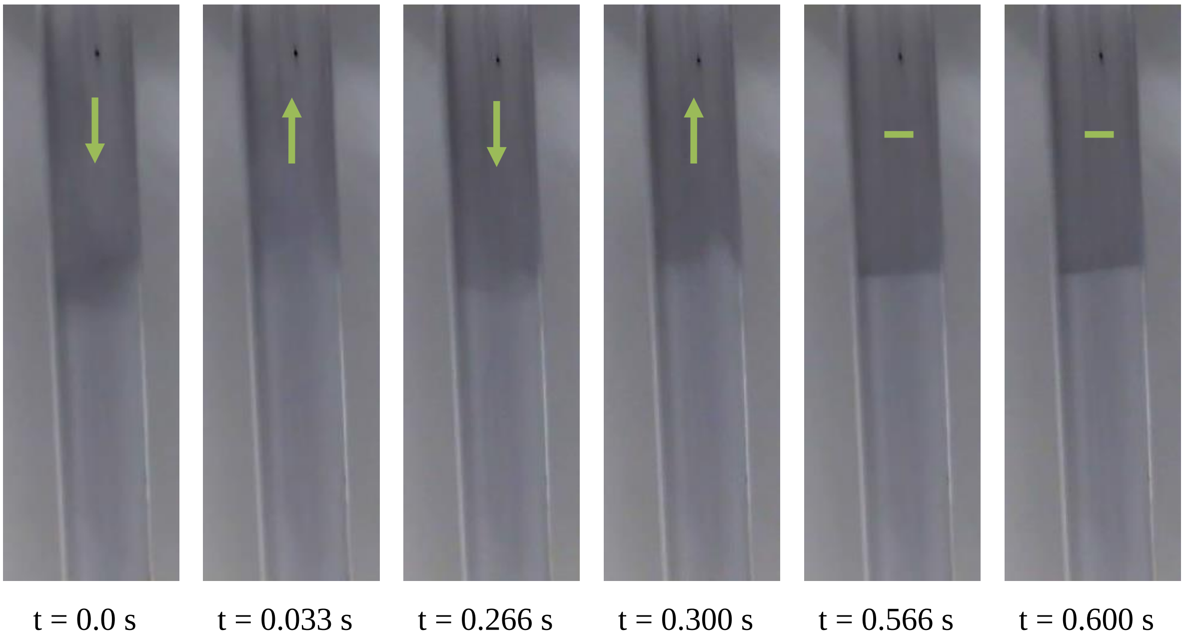

Figure 2: The top meniscus of the fluidized bed captured at 30 Hz; green arrows indicate the direction of oscillation on the free surface; time is shown in the bottom of each image

It was found that the average time period for a single oscillation in the experiments was 0.286 s, which corresponds to a frequency of 3.50 Hz. The length of the wave can be found from the height of the fluidized medium in the tube. It was noted that the height after fluidization was 80 cm. This corresponds to a quarter of a standing wave in a tube with one end closed and the other open; therefore, the complete wavelength of the standing wave is 320 cm. Therefore, the speed of sound is 11.2 m/s.

The results found through experimentation were compared with the speed of sound given by Equation (2). The values of variables used are as follows: the density of alumina silicate particles ρ_s is 3500 kg/m^3, the density of air ρ_g is 1.24 kg/m^3, the temperature of the air T_g is 298 K, (void fraction) ϵ is estimated to be 0.4, and the specific gas constant of the air is 287

J/kg/K. This resulted in the speed of sound in the fluidized medium u_s being equal to 11.23 m/s. Hence, a good agreement between experimental and theoretical results was found.

3 CFD-DEM numerical simulation of speed of sound in a fluidized medium

A computational fluid dynamics-discrete element methods (CFD-DEM) numerical simulation was set up to study the speed of sound in a fluidized medium. The simulated setup is shown below in Figure 3.

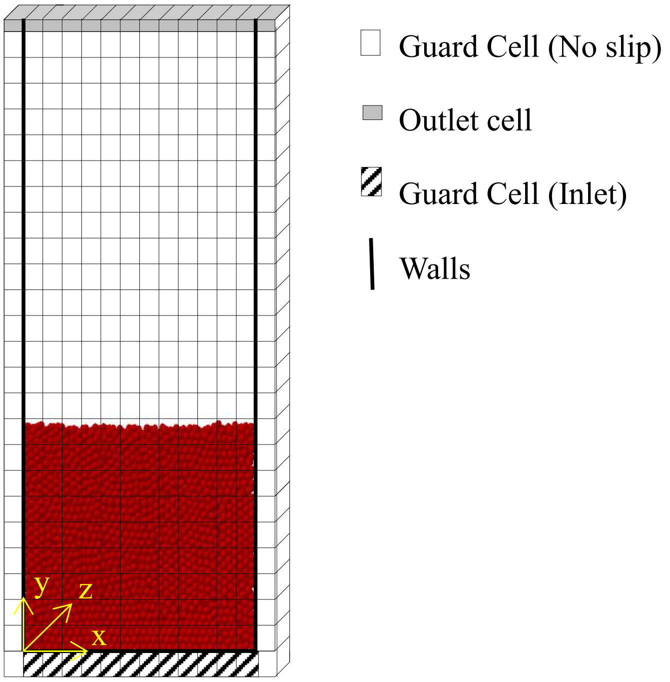

Figure 3: CFD-DEM numerical simulation domain for the study of speed of sound in the fluidized medium; the particles are simulated in three dimensions, whereas fluid is simulated in two dimensions

In this setup, the particles are simulated using a discrete element model as in H. Khawaja (2011); HA Khawaja and Scott (2011), and H. Khawaja (2015). The CFD-DEM model is based on the volume-averaged continuity and momentum equations (Equations (4) and (5)), which are solved using the CFD (computational fluid dynamics) density driven method as discussed in T. B. Anderson and Jackson (1967); Crowe, Sommerfeld, and Tsuji (1998),

$$\frac{\partial(\rho\epsilon)}{\partial t}+\frac{\partial(\rho\epsilon u_k)}{\partial x_k}=0 \tag{4}$$

$$\frac{\partial(\rho\epsilon\, u_i)}{\partial t}+\frac{\partial(\rho\epsilon u_i u_k)}{\partial x_k}=\frac{\partial}{\partial x_k}\epsilon p+\frac{\partial}{\partial x_k}.\epsilon\tau_f-\vec{F}_i+\rho\epsilon g_i \tag{5}$$

where ϵ is the voidage, ρ is the density fluid, u_k is the velocity of the fluid, p is the pressure of the fluid, $\vec{F}_i$ is the interaction force felt by the fluid due to the particles, g_i is the gravity constant and τ_f is the fluid stress tensor. Note that k and i subscripts are Einstein notations (T. B. Anderson & Jackson, 1967). Voidage ϵ is the ratio of the volume of fluid (excluding the particles) to the total volume of a fluid cell. It needs to be accurately computed in a cuboidal domain of CFD with moving spherical particles, as given by (HA Khawaja, Scott, Virk, & Moatamedi, 2012).

The finite volume discretization technique is applied to Equations (4) and (5). This technique is based on conservation of variables; therefore, it ensures that the physical quantities are conserved over the chosen control volumes and the domain as a whole (J. D. Anderson, 1995; Patankar, 1980).

The stability and sensitivity of the solution depend on the time step and cell size, whose values are determined by the Courant-Friedrichs-Lewy (CFL) condition (Courant, Friedrichs, & Lewy, 1928; Hirsch, 2007) as shown in Equation (6),

$$CFL\ Number>\frac{a\,\Delta t}{min(\Delta x,\Delta y,\Delta z)} \tag{6}$$

where Δt is the time step size, $\Delta x, \Delta y, \Delta z$ are the dimensions of the fluid cell and a is the speed of sound in the gas medium.

The interaction force correlations are given by (Beetstra, van der Hoef, & Kuipers, 2007; Di Felice, 1994; Ergun, 1952; Wen & Yu, 1966). By conducting fluidized bed experiments, Müller et al. (2008) compared these correlations and found that the correlation from Beetstra et al.

(2007) is the most promising in the voidage range of $0.3 < \epsilon < 0.5$. This correlation is shown in Equation (7),

$$\beta = A\frac{(1-\epsilon)\mu_f}{\epsilon d_p^2} + B\frac{\mu_f(1-\epsilon)Re}{d_p^2} \tag{7}$$

where β is the drag coefficient, A is shown in Equation (8) and B is shown in Equation (9),

$$A = 180 + \frac{18\epsilon^4}{1-\epsilon}\left(1 + 1.5\sqrt{(1-\epsilon)}\right) \tag{8}$$

$$B = \frac{0.31(\epsilon^{-1} + 3\epsilon(1-\epsilon) + 8.4Re^{-0.343})}{1 + 10^{3(1-\epsilon)}Re^{2\epsilon-2.5}} \tag{9}$$

In CFD-DEM simulations, the interaction force felt by the fluid due to the particles is the sum of the drag on the particles in the particular fluid cell as shown in Equation (10),

$$\vec{F_i} = \frac{1}{(1-\epsilon)V_{cell}}\sum_{i=1}^{n_p}\vec{f_i} \tag{10}$$

where V_{cell} is the volume of the cell, n_p is the number of particles in the cell, $\vec{f_i}$ is the drag force on i particle as shown in Equation (11),

$$\vec{f_i} = V_p\beta(\vec{u}_f - \vec{u}_p) \tag{11}$$

where $\vec{f_i}$ is the force vector felt by the particle due to the fluid drag, V_p is the volume of the particle and β is the drag coefficient computed using the correlation given in Equation (7).

Discrete element modelling (DEM) is based on a Lagrangian approach where each particle's motion is governed by Newton's second law. The linear momentum equation for each particle is,

$$m_p\vec{a}_p = \vec{f}_i + \sum_{contacts}\vec{f}_{contacts} + m_p\vec{g} \tag{12}$$

where m_p is the mass of the particle, $\vec{a}_p$ is the linear acceleration vector, $\vec{f}_i$ is the force on the particles due to the fluid, $\vec{f}_{contact}$ is the force due to the contact with other particles.
The third-order Adams-Bashforth time stepping scheme (Gear, 1971; Hairer, Nørsett, & Wanner, 1993), as shown in Equation (13), is used to advance the fluid as well as the particle variables forward in time.

$$P_{t+1} = P_t + \Delta t \left(\frac{23}{12} dP_{t+1} - \frac{4}{3} dP_t + \frac{5}{12} dP_{t-1} \right) \tag{13}$$

where Δt is the time step size, P_{t+1} is the value of the physical property stepping forward in time, P_t is the value of the physical property before stepping forward in time, and dP is the change in the property. The subscript t in Equation (13) refers to the time step.

Particle-particle contact is solved using soft sphere contact models (Crowe et al., 1998; van der Hoef, Annaland, Deen, & Kuipers, 2008). In the soft contact model, the contact forces are based on a simple linear spring-dashpot model. These models have been used in DEM by (Crowe et al., 1998; Cundall & Strack, 1979; Third, Scott, Scott, & Müller, 2010; Tsuji, Kawaguchi, & Tanaka, 1993; Tsuji, Tanaka, & Ishida, 1992; van der Hoef, van Sint Annaland, & Kuipers, 2004). The contact forces can be divided into normal and tangential forces. The normal contact model is based on the non-linear spring model given by Hertz (Hertz, 1882). The tangential contact model is given by Mindlin and Deresiewicz (1953) and simplified by Tsuji et al. (1992) for DEM. Both models are tested for their suitability for DEM by HA Khawaja and Parvez (2010). The most computationally intensive operation in the CFD-DEM simulation is the search for particle-particle contacts. H. Khawaja (2015) has undertaken a study on the optimization of this algorithm.

The setup is three-dimensional for the particles and two-dimensional for the fluid. The particles are allowed to move in three dimensions, but, due to the narrow domain in the z-direction, as shown in Figure 3, the fluid flow is modeled in the x and y dimensions (this is achieved by setting a single fluid cell in the z-direction). There are 14 cells in the x-direction, of which 12 are computing cells and two are boundary cells. The cells in the y-direction are varied based on the size of the simulation. The physical parameter values set for the CFD-DEM numerical simulation are given in Table 1.

Table 1: Physical parameters set for CFD-DEM numerical simulations

Physical Parameters	*Values*
Fluid pressure	1 bar
Temperature	298.15K
Fluid density	1.13 Kg/m^3
Fluid viscosity	1.8 X 10^{-5} Pa s
Time step size	3.25 X 10^{-7} sec
Number of CFD cells in x-direction	14 (12 computing and 2 boundary cells)
CFD cell size in x-direction	0.45 mm
CFD cell size in y-direction	0.6 mm
Width of domain in z-direction	1.25 mm
Diameter of particles	0.15$\pm$ 0.00625 mm
Density of solid particles	1000 Kg/m^3
Minimum fluidization velocity	0.0085 m/s
Speed of sound in the two-phase medium, from Equation (2)	20.7 m/s
Young modulus of solid particles	1.2 x 10^8 Pa
Poisson ratio of solid particles	0.3
Coefficient of normal restitution for solid particles	0.986
Coefficient of friction	0.1

Four different CFD-DEM numerical simulations were set up with various heights of bed as shown in Table 2.

Table 2: Different sets of CFD-DEM numerical simulations

Test case	*Number of particles*	*Number of cells in y-direction*	*Height of the particles after fluidization (mm)*
1	107800	208	49
2	215320	312	98
3	322480	416	147
4	430360	520	196

The simulation is initialized by randomly placing the particles in the domain. The particles are allowed to fall under gravity to settle down as shown in Figure 3. Then the particles are fluidized to approximately 1.1 times the minimum fluidization velocity (U_{mf}). This is achieved by specifying a rate of change of mass flow rate in the y-direction $\ddot{m}_y$ in the guard (inlet) cells, as shown in Equation (14),

$$
\begin{aligned}
\Delta u_y &= \frac{\ddot{m}_y \Delta t}{\rho_g \Delta x \Delta z} u_y \leq 1.1\ U_{mf} \\
\Delta u_y &= 0 \qquad u_y > 1.1\ U_{mf}
\end{aligned}
\tag{14}
$$

where u_y is the velocity of fluid in the y-direction, Δu_y is the change in fluid velocity in the y-direction, Δx is the dimesion of the fluid cell in the x-direction, Δz is the dimension of the fluid cell in the z-direction, ρ_g is the density of the fluidizing gas and Δt is the time step size. The boundary conditions are specified by specifying walls for the particles in the x, y and z planes as shown in Figure 3 (walls in the z-plane are not visible in Figure 3). The CFD boundary conditions are specified by first setting full slip boundary conditions for the fluid in the cells on either side of the domain in the x-direction. This is achieved by setting the y-velocity in the guard cell equal to one in the closest cell in the x-direction, as shown in Equation (15),

$$
\begin{aligned}
u_{y\ (1,y)} &= u_{y\ (2,y)} \\
u_{y\ (14,y)} &= u_{y\ (13,y)}
\end{aligned}
\tag{15}
$$

where bracketed numbers indicate the position of the cell in the domain and the y coordinate means that it is applicable in all corresponding y-cells except the corner cells. Characteristic boundary conditions are applied to the outlet cells to avoid reflection in pressure signals as discussed in Chung (2010).

Initial attempts to introduce a disturbance into the bed, in which the boundary fluid inflow was perturbed, were unsuccessful. The perturbation quickly damped and did not perturb the relatively massive particles. The given CFD-DEM numerical simulations were performed very close to the minimum fluidization velocity of the particles. Therefore fluid velocity was neither so high that the particles would flow with the fluid nor so low that particles would not be affected at all. Therefore, it was challenging to introduce an appropriate disturbance in such a case. After few trials, it was found that, to introduce an appropriate disturbance, the particles need to be perturbed rather than the fluid. Therefore, the disturbance is introduced by raising the particles in the y-direction by 1.5 mm (10 times the diameter of the particles) and then allowing them to drop under gravity. The sequence of steps taken to introduce this disturbance is illustrated in Figure 4.

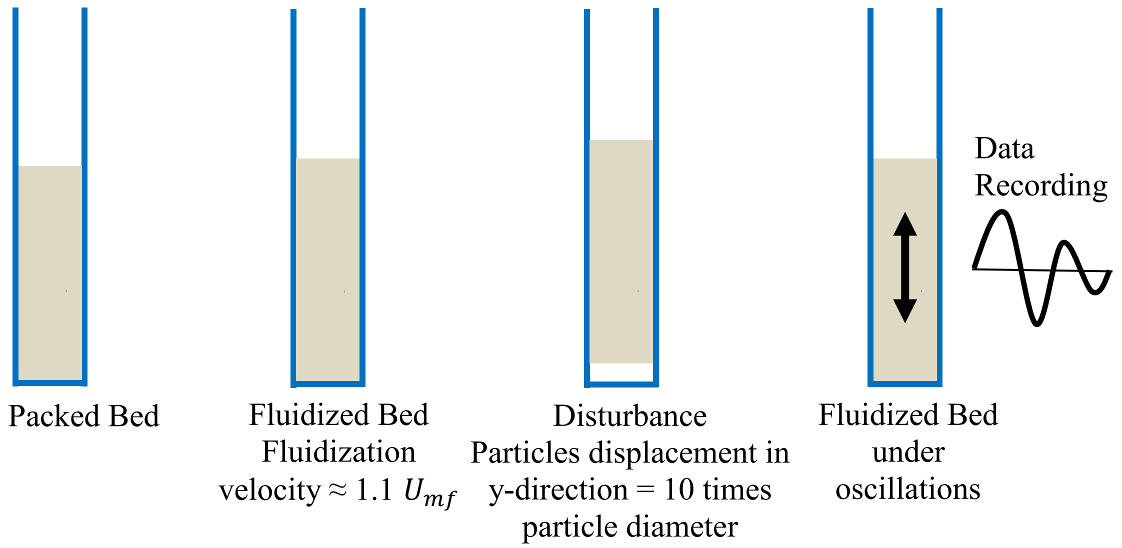

Figure 4: The sequence of steps to generate a disturbance in the fluidized medium

With the drop, the fluidized medium behaves in the same way as discussed earlier in Section 2. This behavior of various physical parameters was recorded and analyzed as discussed in Section 4.

4 Results of CFD-DEM numerical simulation

The results of standing waves from the CFD-DEM numerical simulations in the two-phase medium were investigated by plotting the relevant oscillating physical parameters over time. Fluid pressure and particle velocity were averaged width-wise. The results were averaged in order to reduce the impact of other phenomena in the two-phase medium such as formations of bubbles, their coalescence, their eruption, etc.

It can be observed that the maximum fluctuations in gas pressure occur at the bottom of the bed, whereas the maximum fluctuations in particle velocity occur at the top of the bed (supplementary material). Roy et al. (1990) observed the same trends as shown in Figure 7. These trends can be explained by the fact that particle motion is more constrained at the bottom of the bed in comparison to the particles at the top of the bed. Figure 7 also shows that the highest value of pressure fluctuation occurs at the bottom of the bed, which is in agreement with CFD-DEM numerical simulation results. It can also be observed from Figure 5 that pressure fluctuation is at its peak when the disturbance is introduced at time zero, whereas the particle velocity fluctuation is zero at time zero, as shown in Figure 6. This difference indicates that fluctuations in particle velocity is out of phase by $\frac{\pi}{2}$ from pressure fluctuations.

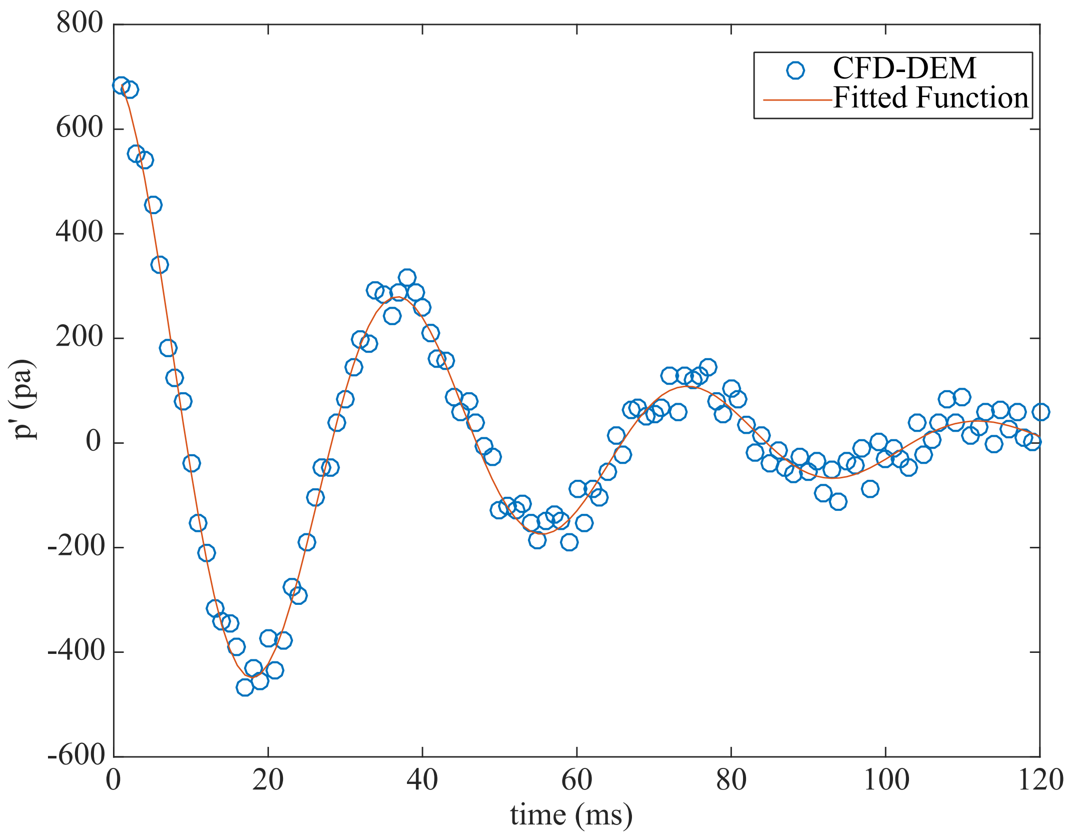

Figure 5: Pressure is plotted against time at 100 mm height in the bed for 430360 particles fluidized bed (test case 4); the red curve shows the fitted function and the blue circles represents the CFD-DEM numerical simulation results

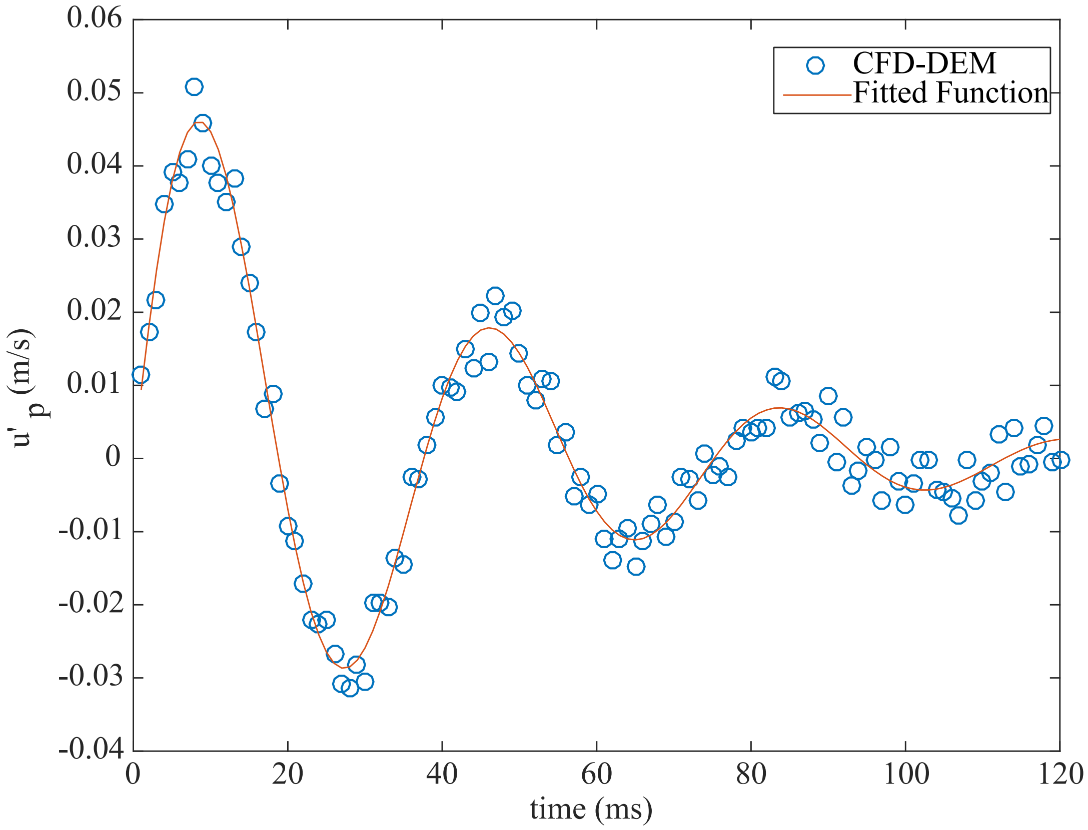

Figure 6: Particle velocity fluctuation plotted against time at 100 mm for 430360 particles fluidized bed (test case 4); the red curve shows the fitted function and the blue circles represents the CFD-DEM numerical simulation results

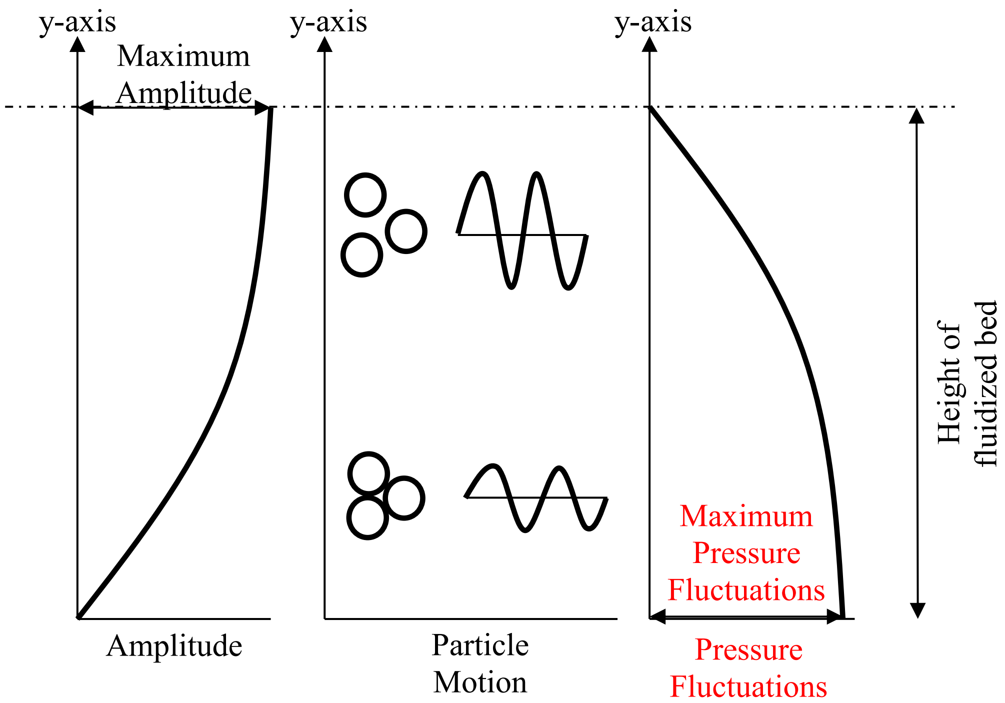

Figure 7: The variation in amplitude of particle velocity and pressure fluctuations of a standing wave in two-phase medium with respect to the height of the bed; amplitude of particle velocity fluctuation is shown on the left, where A is the maximum amplitude and H is height of the bed; oscillation in particle motion is illustrated in the middle; variation in the amplitude of pressure fluctuations is shown on the right [Roy et al. (1990)]

In order to study the interaction between the physical parameters, appropriate functions were fitted in the CFD-DEM numerical simulation results of pressure fluctuation and particle velocity fluctuation. From the fitted equations, it can be seen that the fluctuations in pressure and particle velocity all have the same form, i.e. a sinusoidal variation in time which is damped, multiplied by sinusoidal variation in space; therefore, we can assume a generic function for fluctuation variables as shown,

$$p'(y,t) = P_o e^{-\frac{t}{\tau}} cos(cy) cos(\omega t + \phi_p) \tag{16}$$

$$u'_p(y,t) = U_{p_o} e^{-\frac{t}{\tau}} sin(cy) cos(\omega t + \phi_u) \tag{17}$$

Here P_o , U_{p_o} are the (initial) amplitudes of the pressure and particle velocity fluctuations, respectively; ϕ_p and ϕ_u are the temporal phase shifts, τ is the damping time constant, $c = \frac{\pi}{2h}$, where h is the height of the fluidized medium in the bed, and ω is the angular frequency.

It was found from the fitted equations that the damping time and angular frequency of the oscillations in pressure fluctuation and particle velocity fluctuation are consistent; however, they are out of phase by $\pi/2$. Differences can also be noted in the amplitudes and the time phase angles in the fitted equations.

The values of fitted constants for CFD-DEM cases are given in Table 3.

Table 3: Fitted constants to all test cases according to Equations (16) and (17)

Test case	*Number of particles*	*Height of the particles after fluidization – m*	*Pressure fluctuation amplitude P_o – Pa*	*Particle velocity fluctuation amplitude U_{p_o} – m/s*	*Damping time period τ – s*	*Angular frequency ω – rad/s*
1	107800	0.049	3893	0.298	0.0055	640.5
2	215320	0.098	1962	0.153	0.0129	339.6
3	322480	0.147	1371	0.107	0.0211	222.4
4	430360	0.196	1025	0.0804	0.0397	167.1

5 Analytical study of waves in a fluidized medium

Taking a volume averaged view of the behavior of the fluidized bed, the system can be described by four equations: (1) the volume averaged fluid continuity equation, (2) the volume averaged fluid momentum equation, (3) the volume averaged dispersed phase continuity equation, and (4) the volume averaged dispersed phase momentum equation. These equations are discussed in (H. A. Khawaja, 2015), where (1) and (2) are used as part of the DEM simulation, with the volume averaged particle equations (3 and 4) replaced by a detailed Lagrangian simulation. Here, the volume averaged equations are linearized, and a phasor analysis is applied in an attempt to describe the behavior of the standing waves in the bed, seen both experimentally and in the CFD-DEM simulations. The system is taken to be essentially one-dimensional (i.e. the fluctuations exist in the vertical dimension only), and scaling analysis is used to simplify the equations to a tractable form.

Both the CFD-DEM numerical simulations and experiments (e.g. Roy et al. (1990)) have demonstrated that the presence of particles can alter the speed of sound waves in a two-phase medium. This was also highlighted by Roy et al. (1990) in their derivation of a theoretical relationship for the speed of sound in a two-phase medium. They attributed this behavior to the fluidized phase having not only a large momentum (owing to the motion of the particles), but also a high compressibility (due to the gas). Therefore, any analysis must take into account the particle momentum equation in the y-direction (i.e. vertical). The volume averaged momentum equation for the particle phase (written here on a per particle basis rather than on the per unit volume basis, given by Jackson (2000)) is

$$m_p \frac{\partial u_p}{\partial t} + m_p u_p \frac{\partial u_p}{\partial y} = -k_p\left(u_p - u_g\right) - v_p \frac{\partial p}{\partial y} + m_p g + f \qquad (18)$$

where m_p is the mass of the particle, u_p is the velocity of the particle, k_p is the coefficient of drag force from the fluid, which is a function of local voidage (HA Khawaja et al., 2012), v_p is the volume of the particle, p is the fluid pressure, g is the gravity constant and f is the net force arising from particle contacts. It should be noted that interaction forces here have been explicitly split into terms proportional to the difference between the particle and gas phases. The term f represents the force on the particles from the stresses in the solid phase arising from particle contacts, which, if written on a per unit volume basis, would be equal to the gradient of the solid phase stress tensor. On a per particle basis, this term can be re-written, and in one dimension, as $v_p \nabla S_y$, where S_y is the y component of the particle stress tensor. One of the difficulties in solving the volume averaged equations lies in being able to specify closure relationships for this stress tensor. The simplest closure is used here, which is an analogous form of the stress tensor for the fluid, with a particle pressure, and an effective viscosity for the particle phase [Harris and Crighton (1994)], i.e.

$$f = v_p \frac{\partial}{\partial y}\left(-p_p + \mu_p \frac{\partial u_p}{\partial y}\right) \qquad (19)$$

where μ_p is the effective particle viscosity and p_p is the particle pressure. Harris and Crighton (1994) suggested the particle pressure could be modeled by,

$$p_p = A\left(\frac{1-\epsilon}{\epsilon - \epsilon_{cp}}\right) \qquad (20)$$

where A is a constant, ϵ is the voidage (void fraction) and the subscript cp denotes 'close packing'. This form of equation ensures that the particle pressure becomes infinite when particles are closely packed and reduces to zero when the particles are fully separated. Thus, the particle momentum equation is taken here to be

$$m_p \frac{\partial u_p}{\partial t} + m_p u_p \frac{\partial u_p}{\partial y} = -k_p(u_p - u_g) - v_p \frac{\partial p}{\partial y} + m_p g + v_p \frac{\partial}{\partial y}\left(-p_p + \mu_p \frac{\partial u_p}{\partial y}\right) \tag{21}$$

This equation can be linearized by writing each of the variables (u_p, u_g, p, ϵ) as the sum of the static (i.e. steady state) value, taken here to be at incipient fluidization, plus a small fluctuation. The resulting terms can be substituted in Equation (21). The resulting equations can be linearized and scaled, as discussed in H. A. Khawaja (2013). This analysis results in the correlation of speed of sound and damping time period, as shown in Equations (22) and (23),

$$u_s = \frac{P_o}{(1-\epsilon)\rho_p U_{po}} \tag{22}$$

$$\tau = \frac{\rho_p}{\mu_p c^2} \tag{23}$$

The speed of sound is computed using Equation (22) and compared with those obtained from the CFD-DEM simulations and the theoretical expression given in Equation (2).

Table 4: Speed of sound for test cases given in Table 2; theoretical speed of sound values using Equation (2), CFD-DEM speed of sound values from fitted functions, and CFD-DEM speed of sound values using Equation (22)

Test case	*Theoretical speed of sound using Equation (2) - m/s*	*CFD-DEM speed of sound from fitted functions angular velocity - m/s (percentage difference from theoretical value)*	*CFD-DEM speed of sound using Equation (22) – m/s (percentage difference from theoretical value)*
1	20.7	20.0 (3.4 %)	21.8 (5.3 %)
2	20.7	21.1 (1.9 %)	21.4 (3.4 %)
3	20.7	20.8 (0.5 %)	22.3 (7.7 %)
4	20.7	20.8 (0.5 %)	21.3 (2.9 %)

The results given in Table 4 show that Equation (22) agrees well with both the CFD-DEM fitted function values and the theoretical expression (Equation (2)). It is also observed that the value of $\frac{P_o}{U_{po}}$ is constant. This can be justified by combining Equation (22) with Equation (2). Equation (23) shows that the damping time is a function of the height of the bed, density of particles and bulk particle viscosity. This correlation was used to compute particle viscosity in a fluidized medium for both the simulations here and also in the experiments of Roy et al. (1990). The results are shown in Table 6.

The damping time results of the CFD-DEM test cases are compared using the theoretical relationship given in Roy et al. (1990), as shown in Table 5.

Table 5: Comparison of damping time of oscillations in two-phase medium computed via CFD-DEM numerical simulations and theoretical expression (Equation (3))

Test case	*Height of the bed - mm*	*Theoretical damping time from Equation* (3) *- s*	*CFD-DEM fitted function Damping t - s*	*Percentage difference*
1	49	0.0056	0.0035	37.5 %
2	98	0.0200	0.0129	35.5 %
3	147	0.0467	0.0211	54.8 %
4	196	0.0827	0.0397	52.0 %

The comparison from Table 5 shows a significant difference between the theoretical damping time and the damping time computed via CFD-DEM numerical simulations. Similarly, significant difference is found when this relationship is used against damping time data provided in Roy et al. (1990). The reason that this correlation did not prove to be effective is the fact that the effect in damping due to the particles' contacts was not taken into account in Roy et al. (1990). In contrast, the expression given in Equation (23) includes an effective particle viscosity, which takes into account the damping effect due to particle contacts. Therefore, it is proposed that the damping in a two-phase medium such as a fluidized bed is mainly due to the particles' contacts; however, further study is required in this area.

Table 6: The value of particle viscosity from experimental ([Roy et al. (1990)]) and CFD-DEM results; $\boldsymbol{U_{mf}}$ is the minimum fluidization velocity and $\boldsymbol{u_s}$ is the speed of sound in the fluidized medium

Catalyst; dia. = 70μm, particle density = 1250 kg/m³, U_{mf} = 0.01 m/s, u_s = 15.4 m/s			
Heights (m)	*Time period (s)*	*Damping time period (s)*	*Particle dynamic viscosity (Pa s)*
0.4	0.11	0.06	1350.9
0.6	0.15	0.1	1823.8
0.8	0.21	0.25	1296.9
1	0.26	0.35	1447.4
1.2	0.3	0.43	1696.5
1.4	0.36	0.55	1805.4
1.6	0.43	0.56	2315.9
Glass beads; dia. = 100μm, particle density = 2900 kg/m³, U_{mf} = 0.05 m/s, u_s =11.0 m/s			
Heights (m)	*Time period (s)*	*Damping time period (s)*	*Particle dynamic viscosity (Pa s)*
0.4	0.15	0.08	2350.7
0.6	0.24	0.17	2488.9
0.8	0.29	0.23	3270.5
1	0.38	0.24	4897.2
1.2	0.44	0.29	5836.1
1.4	0.48	0.39	5906.8
1.6	0.53	0.41	7338.6
Vermiculite; dia. = 220μm, particle density = 384 kg/m³, U_{mf} = 0.025 m/s, u_s =23.3 m/s			
Heights (m)	*Time period (s)*	*Damping time period (s)*	*Particle dynamic viscosity (Pa s)*
0.4	0.07	0.05	498.0
0.6	0.1	0.08	700.3
0.8	0.14	0.1	996.0
1	0.17	0.13	1197.1
1.2	0.21	0.16	1400.7
1.4	0.23	0.21	1452.5
1.6	0.28	0.24	1660.0
CFD-DEM; dia. = 150μm, particle density = 1000 kg/m³, U_{mf} = 0.0085 m/s, u_s =20.7 m/s			
Heights (m)	*Time period (s)*	*Damping time period (s)*	*Particle dynamic viscosity (Pa s)*
0.049	0.00981	0.0055	278.0
0.098	0.0185	0.0129	301.7
0.147	0.02825	0.0211	415.1
0.196	0.0376	0.0397	503.9

The computed particle viscosities are much higher than those reported by Hagyard and Sacerdote (1966). However, Hagyard and Sacerdote (1966) showed that the particle viscosity increases asymptotically when close to minimum fluidization; therefore, the found values are reasonable, considering that the tests were performed very close to minimum fluidization. Particle viscosity is because of particles contacts hence its value rises as hydrostatic pressure rises in the fluidized bed.

6 Conclusions

In this work, sound waves were studied in a fluidized medium using CFD-DEM simulations. The following conclusions can be drawn from this study:

- The theoretical relationship for speed of sound in a two-phase medium given by Roy et al. (1990) was validated by the CFD-DEM numerical simulations.
- The linearized equations were used to show that the speed of sound in a two-phase medium can be linked to physical properties of the particles and the amplitudes of fluctuations in pressure and particle velocity. Since the speed of sound in a two-phase medium is constant (Roy et al. (1990)), it was also shown that the ratio of the amplitude of the fluctuations in pressure and particle velocity is also constant. This was also observed in CFD-DEM simulations.
- The most significant effect in terms of damping was the particle viscous term. Previous work by Roy et al. (1990) had neglected this effect, with the consequence that they were not able to describe the damping accurately. Using the expressions derived from the linear analysis, it was possible to compute the particle dynamic viscosity for the experiments from Roy et al. (1990) and CFD-DEM test cases.

7 Acknowledgements

The author acknowledges the support of Dr. Stuart A. Scott, Department of Engineering, University of Cambridge, UK and Prof. John F. Davidson, Department of Chemical Engineering, University of Cambridge, UK.

List of references

Anderson, J. D. (1995). *Computational fluid dynamics: the basics with applications*: McGraw-Hill.

Anderson, T. B., & Jackson, R. (1967). Fluid Mechanical Description of Fluidized Beds. Equations of Motion. *Industrial & Engineering Chemistry Fundamentals, 6*(4), 527-539. doi:10.1021/i160024a007

Beetstra, R., van der Hoef, M. A., & Kuipers, J. A. M. (2007). Numerical study of segregation using a new drag force correlation for polydisperse systems derived from lattice-Boltzmann simulations. *Chemical Engineering Science, 62*(1–2), 246-255. doi:10.1016/j.ces.2006.08.054

Bi, H. T. (2007). A critical review of the complex pressure fluctuation phenomenon in gas–solids fluidized beds. *Chemical Engineering Science, 62*(13), 3473-3493. doi:10.1016/j.ces.2006.12.092

Bi, H. T., Grace, J. R., & Zhu, J. (1995). Propagation of pressure waves and forced oscillations in gas-solid fluidized beds and their influence on diagnostics of local hydrodynamics. *Powder Technology, 82*(3), 239-253. doi:10.1016/0032-5910(94)02929-i

Cahan, D. (1990). From dust figures to the kinetic theory of gases: August Kundt and the changing nature of experimental physics in the 1860s and 1870s. *Annals of science, 47*(2), 151-172.

Campbell, I. J., & Pitcher, A. S. (1958). Shock Waves in a Liquid Containing Gas Bubbles. *Proceedings of the Royal Society of London. Series A. Mathematical and Physical Sciences, 243*(1235), 534-545. doi:10.1098/rspa.1958.0018

Chung, T. J. (2010). *Computational Fluid Dynamics*: Cambridge University Press.

Courant, R., Friedrichs, K., & Lewy, H. (1928). Über die partiellen Differenzengleichungen der mathematischen Physik. *Mathematische Annalen, 100*(1), 32-74. doi:10.1007/bf01448839

Crowe, C. T., Sommerfeld, M., & Tsuji, Y. (1998). *Multiphase Flows With Droplets and Particles*: CRC Press.

Cundall, P. A., & Strack, O. D. L. (1979). A discrete numerical model for granular assemblies. *Geotechnique, 29*(1), 47-65. doi:citeulike-article-id:9245301

Di Felice, R. (1994). The voidage function for fluid-particle interaction systems. *International Journal of Multiphase Flow, 20*(1), 153-159. doi:10.1016/0301-9322(94)90011-6

Ergun, S. (1952). Fluid flow through packed columns. *Chem. Process Eng. London, 1*, 89-94.

Gear, C. W. (1971). *Numerical initial value problems in ordinary differential equations*: Prentice-Hall.

Hagyard, T., & Sacerdote, A. M. (1966). Viscosity of Suspensions of Gas-Fluidized Spheres. *Industrial & Engineering Chemistry Fundamentals, 5*(4), 500-508. doi:10.1021/i160020a012

Hairer, E., Nørsett, S. P., & Wanner, G. (1993). *Solving Ordinary Differential Equations: Nonstiff problems*: Springer.

Harris, S. E., & Crighton, D. G. (1994). Solitons, solitary waves, and voidage disturbances in gas-fluidized beds. *Journal of Fluid Mechanics*, *266*, 243-276.

Hertz, H. (1882). Über die Berührung fester elastischer Körper. *J. Reine Angew. Mat.*(92), 156–171.

Hirsch, C. (2007). *Numerical Computation of Internal and External Flows: Fundamentals of Computational Fluid Dynamics*: Elsevier/Butterworth-Heinemann.

Jackson, R. (2000). *The Dynamics of Fluidized Particles*: Cambridge University Press.

Khawaja, H. (2011). CFD-DEM Simulation of Minimum Fluidisation Velocity in Two Phase Medium. *The International Journal of Multiphysics, 5*(2), 89-100. doi:10.1260/1750-9548.5.2.89

Khawaja, H. (2015). CFD-DEM and Experimental Study of Bubbling in a Fluidized Bed. *The Journal of Computational Multiphase Flows, 7*(4), 227-240.

Khawaja, H., & Parvez, K. (2010). Validation of normal and frictional contact models of spherical bodies by FEM analysis. *The International Journal of Multiphysics, 4*(2), 175-185.

Khawaja, H., & Scott, S. (2011). CFD-DEM Simulation of Propagation of Sound Waves in Fluid Particles Fluidised Medium. *The International Journal of Multiphysics*, *5*(1), 47-60.

Khawaja, H., Scott, S., Virk, M., & Moatamedi, M. (2012). Quantitative Analysis of Accuracy of Voidage Computations in CFD-DEM Simulations. *The Journal of Computational Multiphase Flows*, *4*(2), 183-192.

Khawaja, H. A. (2013). *CFD-DEM simulations of two phase flow in fluidised beds.* (PhD Thesis), University of Cambridge, Cambridge, UK.

Khawaja, H. A. (2015). Review of the phenomenon of fluidization and its numerical modelling techniques. *The International Journal of Multiphysics, 9*(4), 397-408. doi:10.1260/1750-9548.9.4.397

Kunii, D., & Levenspiel, O. (1991). *Fluidization Engineering*: Butterworth-Heinemann.

Lamb, H. (1963). *Hydrodynamics (6th Edition)*. Cambridge: Cambridge University Press.

Mallock, A. (1910). The Damping of Sound by Frothy Liquids. *Proceedings of the Royal Society of London. Series A, 84*(572), 391-395. doi:10.1098/rspa.1910.0085

Mindlin, R. D., & Deresiewicz, H. (1953). Elastic Spheres in Contact Under Varying Oblique Forces. *J. of Appl. Mech., 20*, 327. doi:citeulike-article-id:7798914

Müller, C. R., Holland, D. J., Sederman, A. J., Scott, S. A., Dennis, J. S., & Gladden, L. F. (2008). Granular temperature: Comparison of Magnetic Resonance measurements with Discrete Element Model simulations. *Powder Technology, 184*(2), 241-253. doi:10.1016/j.powtec.2007.11.046

Patankar, S. V. (1980). *Numerical Heat Transfer and Fluid Flow*: Taylor & Francis.

Roy, R., Davidson, J. F., & Tuponogov, V. G. (1990). The velocity of sound in fluidised beds. *Chemical Engineering Science, 45*(11), 3233-3245. doi:10.1016/0009-2509(90)80216-2

Tangren, R. F., Dodge, C. H., & Seifert, H. S. (1949). Compressibility Effects in Two-Phase Flow. *Journal of Applied Physics, 20*(7), 637-645.

Third, J., Scott, D., Scott, S., & Müller, C. (2010). Tangential velocity profiles of granular material within horizontal rotating cylinders modelled using the DEM. *Granular Matter, 12*(6), 587-595. doi:10.1007/s10035-010-0199-2

Tsuji, Y., Kawaguchi, T., & Tanaka, T. (1993). Discrete particle simulation of two-dimensional fluidized bed. *Powder Technology, 77*(1), 79-87. doi:10.1016/0032-5910(93)85010-7

Tsuji, Y., Tanaka, T., & Ishida, T. (1992). Lagrangian numerical simulation of plug flow of cohesionless particles in a horizontal pipe. *Powder Technology, 71*(3), 239-250. doi:10.1016/0032-5910(92)88030-l

Turton, R., Fitzgerald, T. J., & Levenspiel, O. (1989). An experimental method to determine the heat transfer coefficient between fine fluidized particles and air via changes in magnetic properties. *International Journal of Heat and Mass Transfer, 32*(2), 289-296. doi:10.1016/0017-9310(89)90176-2

van der Hoef, M. A., Annaland, M. V., Deen, N. G., & Kuipers, J. A. M. (2008). Numerical simulation of dense gas-solid fluidized beds: A multiscale modeling strategy *Annual Review of Fluid Mechanics* (Vol. 40, pp. 47-70). Palo Alto: Annual Reviews.

van der Hoef, M. A., van Sint Annaland, M., & Kuipers, J. A. M. (2004). Computational fluid dynamics for dense gas–solid fluidized beds: a multi-scale modeling strategy. *Chemical Engineering Science, 59*(22–23), 5157-5165. doi:10.1016/j.ces.2004.07.013

Wen, C. Y., & Yu, Y. H. (1966). Mechanics of fluidization. *Chem. Eng. Prog. Symp. Series.*(62), 100–111.